Energy stored in nanoscale water capillary bridges formed between chemically heterogeneous surfaces with circular patches

Bin-Ze Tang(唐宾泽), Xue-Jia Yu(余雪佳), Sergey V. Buldyrev, Nicolas Giovambattista, Li-Mei Xu(徐莉梅)

Citation: Chin. Phys. B . 2020, 29(11): 114703 . **doi:** 10.1088/1674-1056/abb664
Journal homepage: http://cpb.iphy.ac.cn; http://iopscience.iop.org/cpb

What follows is a list of articles you may be interested in

Density and temperature reconstruction of a flame-induced distorted flow field based on background-oriented schlieren (BOS) technique

Guang-Ming Guo(郭广明), Hong Liu(刘洪)

Chin. Phys. B . 2017, 26(6): 064701 . **doi:** 10.1088/1674-1056/26/6/064701

Three-dimensional turbulent flow over cube-obstacles

Hao Lu(卢浩), Wen-Jun Zhao(赵文君), Hui-Qiang Zhang(张会强), Bing Wang(王兵), Xi-Lin Wang(王希麟)

Chin. Phys. B . 2017, 26(1): 014703 . **doi:** 10.1088/1674-1056/26/1/014703

Characteristics and generation of elastic turbulence in a three-dimensional parallel plate channel using direct numerical simulation

Hong-Na Zhang(张红娜), Feng-Chen Li(李凤臣), Xiao-Bin Li(李小斌), Dong-Yang Li(李东阳), Wei-Hua Cai(蔡伟华), Bo Yu(宇波)

Chin. Phys. B . 2016, 25(9): 094701 . **doi:** 10.1088/1674-1056/25/9/094701

SPECIAL TOPIC — Water at molecular level

Energy stored in nanoscale water capillary bridges formed between chemically heterogeneous surfaces with circular patches*

Bin-Ze Tang(唐宾泽)[1,†], Xue-Jia Yu(余雪佳)[1,†], Sergey V. Buldyrev[2,‡], Nicolas Giovambattista[3,4,§], and Li-Mei Xu(徐莉梅)[1,5,¶]

[1] International Center for Quantum Materials, School of Physics, Peking University, Beijing 100871, China
[2] Department of Physics, Yeshiva University, 500 West 185th Street, New York, NY 10033, United States
[3] Department of Physics, Brooklyn College of the City University of New York, Brooklyn, New York 11210, United States
[4] Ph.D. Programs in Chemistry and Physics, The Graduate Center of the City University of New York, New York, NY 10016, United States
[5] Collaborative Innovation Center of Quantum Matter, Beijing 100871, China

(Received 27 July 2020; revised manuscript received 1 September 2020; accepted manuscript online 9 September 2020)

The formation of nanoscale water capillary bridges (WCBs) between chemically heterogeneous (patchy) surfaces plays an important role in different scientific and engineering applications, including nanolithography, colloidal aggregation, and bioinspired adhesion. However, the properties of WCB of nanoscale dimensions remain unclear. Using molecular dynamics simulations, we investigate the geometrical and thermodynamic properties of WCB confined between chemically heterogeneous surfaces composed of circular hydrophilic patches on a hydrophobic background. We find that macroscopic capillary theory provides a good description of the WCB geometry and forces induced by the WCB on the confining surfaces even in the case of surface patches with diameters of only 4 nm. Upon stretching, the WCB contact angle changes from hydrophobic-like values ($\theta > 90^\circ$) to hydrophilic-like values ($\theta < 90^\circ$) until it finally breaks down into two droplets at wall separations of $\sim$ 9–10 nm. We also show that the studied nanoscale WCB can be used to store relevant amounts of energy E_P and explore how the walls patch geometry can be improved in order to maximize E_P. Our findings show that nanoscale WCB can, in principle, be exploited for the design of clean energy storage devices as well as actuators that respond to changes in relative humidity. The present results can also be of crucial importance for the understanding of water transport in nanoporous media and nanoscale engineering systems.

Keywords: water capillary bridge, energy density, morphology transition, hydrophilicity

PACS: 47.55.nk, 68.35.Md, 61.30.Hn, 82.30.Rs **DOI:** 10.1088/1674-1056/abb664

1. Introduction

Water capillary bridges (WCBs) are not only common in the macroscopic world but exist widely at the nanoscale. For example, at large humidity conditions, WCB can spontaneously form between the tip of an atomic force microscope (AFM) and the sample being studied,[1–3] affecting the corresponding AFM measurement. WCB can also mediate the interactions between nanoparticles and solutes in general. For example, in the case of polymer systems, WCB can induce the self-assembling of the polymers.[4,5] The study of capillary bridges has mainly been focused on the case where the confining surfaces are homogeneous.[6–11] However, a few recent computational studies have considered the role of surface chemical heterogeneity on the geometric and thermodynamic properties of capillary bridge.[12,13] These heterogeneous surfaces are usually composed of hydrophilic and hydrophobic regions, for example, hydrophobic surfaces decorated with stripe-like hydrophilic patches. It has been shown that macroscopic capillarity theory (macroscopic thermodynamics)[14,15] works successfully even in the case of patchy surfaces with nanoscale patch sizes and walls separations.[13,16] However, these studies are limited by the patch geometry considered and it is not clear what is the role of path dimensions and shape on the properties of the capillary bridges considered (e.g, capillary bridge profile, energy, force induced on the confining surfaces, etc). The properties of nanoscale WCB confined by chemically heterogeneous surfaces are challenging to predict theoretically.[17–19] Understanding how the surface patch geometry affects the properties of capillary bridges can help engineers to design heterogeneous surfaces to improve chip self-alignment during pickup for the fabrication of chip arrays,[20] and micro-transfer process in printing process.[21,22]

In a recent molecular dynamics simulations study, we[13]

*Project support by the National Natural Science Foundation of China (Grant Nos. 11525520 and 11935002) and the National Key Research and Development Program of China (Grant No. 2016YFA0300901).

†These authors contributed equally.
‡Corresponding author. E-mail: buldyrev@yu.edu
§Corresponding author. E-mail: ngiovambattista@cuny.edu
¶Corresponding author. E-mail: limei.xu@pku.edu.cn

showed that the properties of a translationally-symmetric (TS) nanoscale WCB formed between two flat surfaces with a stripe-like hydrophilic patch can be described remarkably well by capillary theory. Moreover, it was found that, upon stretching, the WCB can stored relative large energy densities. The stored energy densities in such WCB are comparable to the energy harvested by water responsive materials that work under changes in relative humidity.[23] In this work, we extend the previous study, based on TS (i.e., stripe-like) patches, and explore how the geometry of the hydrophilic patch can be modified in order to optimize the energy stored in the corresponding WCB. Specifically, here we consider axis-symmetry (AS) WCB formed between circular patches (see Fig. 1) of different size, and test whether the resulting WCB can store more energy than the TS WCB. In addition, we test whether capillarity theory applies when the surfaces are decorated with circular patches of nanoscale dimensions. Our results suggest that macroscopic capillary theory works remarkably well for the case of AS WCB formed between surfaces separated by $h > 3.5$ nm even for patches as small as 4 nm in diameter. Upon stretching, the contact angle of the WCB changes from hydrophilic ($\theta < 90^\circ$), at small h, to hydrophobic ($\theta > 90^\circ$), at large h. In addition, we find that the minimum value of θ decreases as the patch diameter d increases. These effects alter the energy stored in the corresponding WCB. For example, our MD simulations show that the energy stored in the WCB can be optimized by increasing the size of the patch. In addition, we find that the heterogeneous surfaces with hydrophilic patches increase the stability of the WCB. Specifically, WCB formed between hydrophobic surfaces becomes unstable (break) at $h = 7.5$ nm while in the presence of hydrophilic circular patches, the WCB becomes unstable at $h \sim 9.5$ nm. These results can be of crucial importance for the understanding of water transport in nanoporous media[24] and oil resource exploitation.[25]

This work is organized as follows. In Section 2, we provide the computer simulation details and methods employed. In Section 3, we present the simulation results focused on the WCB profile, force induced by WCB on the wall, and energy stored in WCB. A summary is included in Section 4.

2. Methods

We perform molecular dynamics (MD) computer simulations of an AS WCB composed of $N = 3375$ water molecules expanding between two identical silica-based surfaces. The surfaces are hydrophobic (non-hydroxylated silica) and are decorated with a circular hydrophilic patch (hydroxylated silica); see Fig. 1. The surfaces are oriented parallel to each other, perpendicular to the z-axis, in a mirror configuration

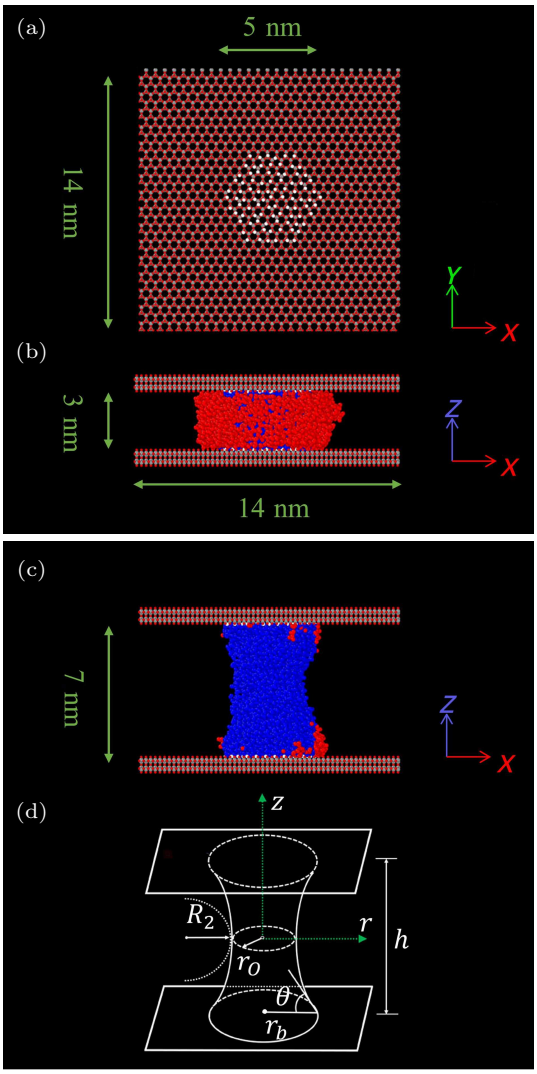

Fig. 1. (a) Top view of one of the chemically heterogeneous surfaces considered in this work. The surface is hydrophobic with a silica-based structure and is hydroxylated over a region of diameter $d = 5$ nm. The Si, O, and H atoms are denoted by gray, red, and white spheres, respectively. The surfaces expand across the simulation box; periodic boundary conditions apply along the x- and y-axes. (b) and (c) Snapshots of a water capillary bridge formed between two surfaces separated by a distance $h = 3$ and 7 nm, respectively. Water molecules within the capillary bridge that are confined between the hydrophilic patches of the surfaces are colored in blue; water molecules located beyond the hydrophilic patches are shown in red. (d) Illustration of a capillary bridge with the main parameters employed in this work. h is the wall separations, r_0 and R_2 are the curvature radii of the capillary bridge, r_b is the corresponding base radius, and θ is the water contact angle.

and the WCB expands between the hydrophilic patch of the walls. We consider different circular hydrophilic patches with diameters ranging from $d = 4$ nm to 7 nm. To be noticed, the hexagonal patch shown in Fig. 1(a) is an approximation to the circular patch due to the limitation of patch size and surface structure. For larger d, the patch tends to be more like a circle. Details of the surface structure and water–wall interactions can be found in Ref. [26]. Briefly, the O and Si atoms of the walls are fixed during the MD simulation; the H atoms are able to move on a plane parallel to the walls. Only Si and O atoms interact with water O atoms via Lennard–Jonnes interactions. Atoms in the wall have no partial charge with ex-

ception of the surface silanol groups of the hydrophilic patch. Hence, only the surface Si, O, and H atoms of the hydrophilic patch interact with water via Coulombic interactions (and can forms hydrogen bonds with water). Water molecules are represented by the SPC/E water model.[27] The hydrophobic regions of the walls are characterized by a water contact angle of $\theta \approx 108^\circ$; the contact angle of water in contact with the hydrophilic patch is $\theta \approx 0^\circ$.[28,29] The surfaces have dimensions of $L_x = L_y = L = 14$ nm and expand across the simulation box. The simulation box is cubic with side length L and periodic boundary conditions are applied along the x, y, and z directions; additional MD simulations details can be found in Refs. [16,28].

All our MD simulations are performed using the LAMMPS software package[30] at constant volume V, number of water molecules N, and temperature $T = 300$ K. The simulation time step is 0.001 ps and the total simulation time at a given (N, V, T) is 5 ns. Data for analysis are collected within the last 2 ns of the trajectory and snapshots of the system are saved every 1 ps. MD simulations are performed at $h = 2.5$ nm, 3.0 nm, 3.5 nm, ..., 10 nm. We first perform MD simulations at wall separations $h = 5$ nm and the WCB is then compressed and stretched to $h = 4.5$ nm and 5.5 nm along the z-axis (in these processes, the wall separation is reduced/increased by 0.02 nm and relaxed for 1 ps). After the new MD simulations are completed at $h = 4.5$ nm, 5.5 nm, the process is repeated until the new desired values of h are reached.

Capillarity theory predicts that the profile of an AS capillary bridge expanding along the z is given by

$$\frac{\mathrm{d}z}{\mathrm{d}r} = \pm \frac{\left|H\left(r^2 - r_0^2\right) + r_0\right|}{\sqrt{r^2 - \left[H\left(r^2 - r_0^2\right) + r_0\right]^2}}, \tag{1}$$

where $r(z)$ is the profile of the AS capillary bridge, r_0 is the corresponding neck radius (at $z = 0$); see Fig. 1(c). In this expression, $H = \frac{1}{2}(\frac{1}{r_0} + \frac{1}{R_2})$ is the capillary bridge surface curvature and R_2 is the curvature radius which is positive for convex and negative for concave bridge. Part of this work consists of testing whether Eq. (1) is consistent with the results obtained from MD simulations. The WCB profile from our MD simulations is obtained as follows (see also Ref. [28]). We first divide the WCB into slabs of thickness $\delta = 0.5$ nm. The slabs are located at $z_i = h/2 - 0.25$ nm, $h/2 - 2 \times 0.25$ nm, ..., $-(h/2 - 0.25)$ nm and are parallel to the walls. Then, we calculate the average density of water within slab i as a function of r, where r is the distance to the axis passing through the center of mass of the WCB (see Fig. 1(d)). The radius of the bridge r_i within the i-th slab is determined by the liquid–vapor boundary where the density of liquid is set to $\rho_0 = 0.2$ g/cm^3. The set of values (z_i, r_i) is then fitted using Eq. (1) to obtain $r(z)$. We note that $r(z)$ can be obtained by fitting (i) all the values (z_i, r_i), or (ii) those excluding the data points (z_i, r_i) closest to each surface (two data points in total). This is because, at the nanoscale, the density of water within the slabs next to the surfaces may be underestimated due to an empty space of ~ 0.1–0.2 nm between the water molecules and the surface atoms (see Ref. [31]), and the water layer near heterogeneous boundary may have different structure which affects the fitting results.

3. Results

3.1. Water capillary bridge profile

The density profile of the WCB studied is shown in Fig. 2. Circles are the radius of the WCB at height z_i directly obtained form the MD simulations (see Section 2). The solid and dashed lines are the theoretical profiles $r(z)$ predicted by capillarity theory. Specifically, the dashed lines are the best fit to all the MD simulation data points (circle) using Eq. (1). Solid lines are the best fit of the MD data points when the closest points to the upper and lower surfaces are removed. Figure 2 clearly shows that capillarity theory predicts successfully the profile of the WCB for all wall separation h and surface path diameter d. In agreement with our previous study, our MD simulations show that capillarity theory can be extended down to WCB of ~ 2.5 nm in length. In addition, we find that capillarity theory can also be extended down to hydrophilic patches of only 4 nm in diameter. We stress that these are very small dimensions, comparable to the thickness of the liquid–vapor interface (≈ 1 nm). Interestingly, it follows from Fig. 2 that, contrary to the case of homogeneous surfaces, WCB confined by patchy surface of dimensions commensurate to the WCB, are not characterized by a single contact angle. Indeed, the contact angle of of WCB varies considerably, from hydrophobic-like ($\theta > 90^\circ$) to hydrophilic-like ($\theta < 90^\circ$). This results in WCB that are convex at small h, and concave at large h.[17,32] Notably, in spite of the morphology change of WCB, the bridge volume tends to be a constant regardless of the patch size and walls separation.

The WCB geometry can also be characterized by its base radius next to the surface $r_\mathrm{b} = r(\pm h/2)$ and the contact angle θ of water (see Fig. 1(d)). Figure 3 shows $\theta(h)$ and $r_\mathrm{b}(h)$ corresponding to the theoretical profiles shown by the solid line in Fig. 2. For small values of h, the contact angle θ of the WCB is about 105° which is close to the contact angle of water in contact with the hydrophobic, homogeneous silica walls.[28] As h increases, θ initially decreases with h and reaches a minimum value that depends on d. Upon further increase in h, θ increases again. In contrast, the contact angles of the WCB are constant when the surfaces are homogeneous.[28] The anomalous behavior of $\theta(h)$ becomes more pronounced as the patch size increases.

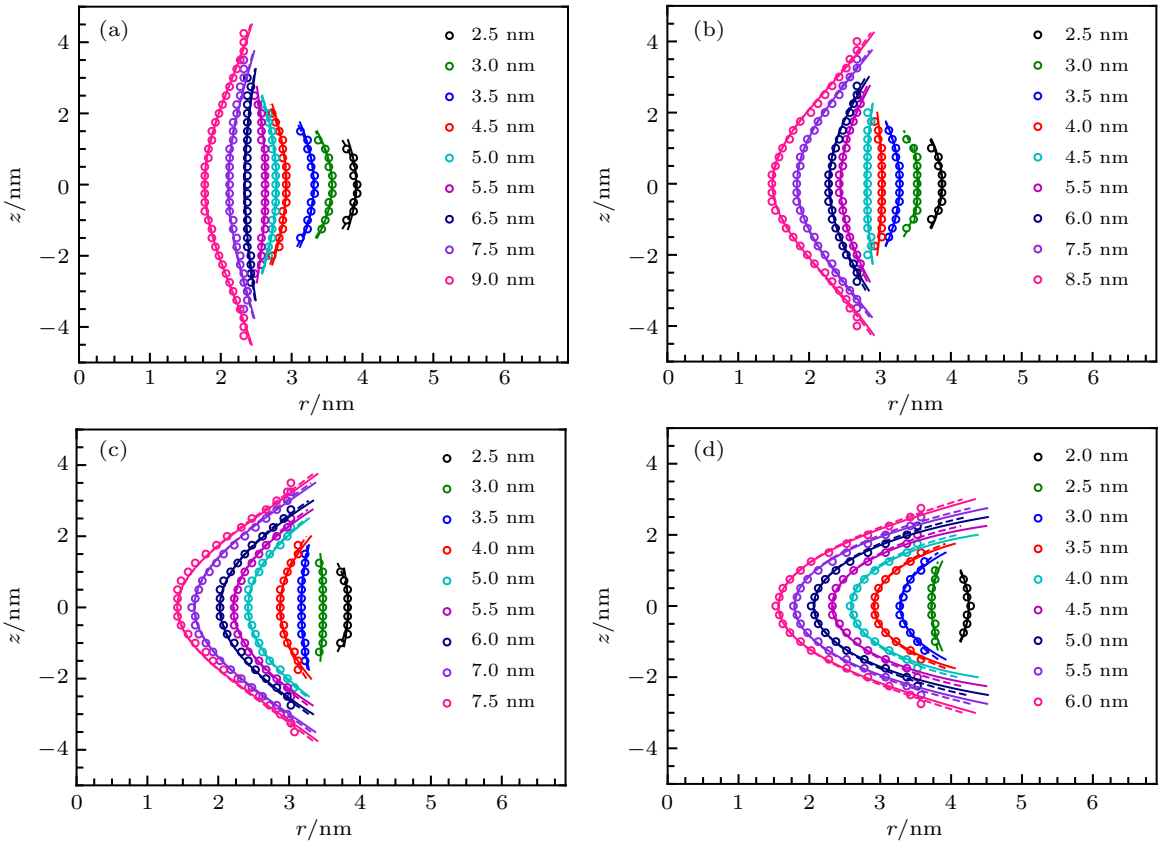

Fig. 2. Profiles of the water capillary bridges as function of separation h for surface patch diameter (a) $d = 4$ nm, (b) $d = 5$ nm, (c) $d = 6$ nm, and (d) $d = 7$ nm. The water capillary bridge profiles obtained from the MD simulations are denoted by open circles. Solid and dashed lines represent the capillary bridge profiles predicted by capillarity theory and obtained by fitting the MD data (circles) using Eq. (1), respectively. The dashed line is obtained by considering all the MD data points (circles) in the fitting procedure. The solid line is the best fit obtained when the points closest to the upper and lower surfaces are omitted in the fitting procedure.

The behavior of $r_b(h)$ is shown in Fig. 3(b). For all patch dimensions, r_b varies with h but it remains $> d/2$. As one can see from Fig. 2, CT overestimates the base radius compared to the data obtained by the MD simulations (circles in Fig. 2). Nevertheless, the base radii obtained from MD simulations are still larger than $d/2$ by about 0.05–0.1 nm. This indicates that at all wall separations, the bridge expands over the whole patch surface.[33] Hence, in agreement with the previous work,[13] the presence of the hydrophilic patch ($\theta = 0°$) allows water molecules to somehow wet the hydrophobic regions surrounding the hydrophilic patch.

In order to carry out a more delicate investigation of the patch boundary ("pinning") effect, we use macroscopic CT to show the behavior of $\theta(\eta, \delta)$, where $\eta = \dfrac{h}{2V^{1/3}}$, $\delta = \dfrac{r_b}{V^{1/3}}$, and V and r_b are the volume and base radius of the bridge, respectively. As shown in Fig. 3(c), we can plot a $\theta(\eta)$ for each δ. The circles in Fig. 3(c) are obtained from Fig. 3(a) where we fix the bulk water ($N = 3375$) volume $V = 101$ nm^3 as a constant. For the value of δ in each group, we set $r_b = d/2 + 0.1$ nm where d corresponds to the patch diameter in our simulation. The dashed lines in Fig. 3(c) are the prediction results from macroscopic CT.[15] The discrepancies between the circles and lines mainly come from two sources. The first one is the slip-out of the WCB which occurs roughly at $\theta > 90°$. The second one is that the contact area in our simulations fitting is always larger than our CT calculation where we assume that the base is constant and equal to the hydrophilic patch size. We conjecture that the ridged water layer near the walls may cause these results. As shown in Fig. 2, the profiles develop inflection points near the wall, the existence of which in the stable bridge profile contradicts the CT.[34,35] We note that the inflection points were not observed in the MD simulations of the liquid bridges between the homogeneous walls.[16,28] We conjecture that this could be because there is a monomolecular layer of structured water near the polar interface which makes macroscopic capillary theory inapplicable at small distances from the wall. Because of the large polarity of the hydrophilic patch, the profile $r(z)$ of the WCB main body crosses the patch boundary at the height $z = h/2 - \Delta h$, which more or less coincides with the inflection point. On the other hand, the fitting which describes the WCB profile main body (without the monomolecular layer) part gives a good prediction to the thermodynamic behavior of WCB (see Subsection 3.2). We note that, in spite of the discrepancies, CT can give a qualitative description of our nanoscale WCBs (see $d = 5$ nm, 6 nm) including a non-monotonic behavior of $\theta(\eta)$.

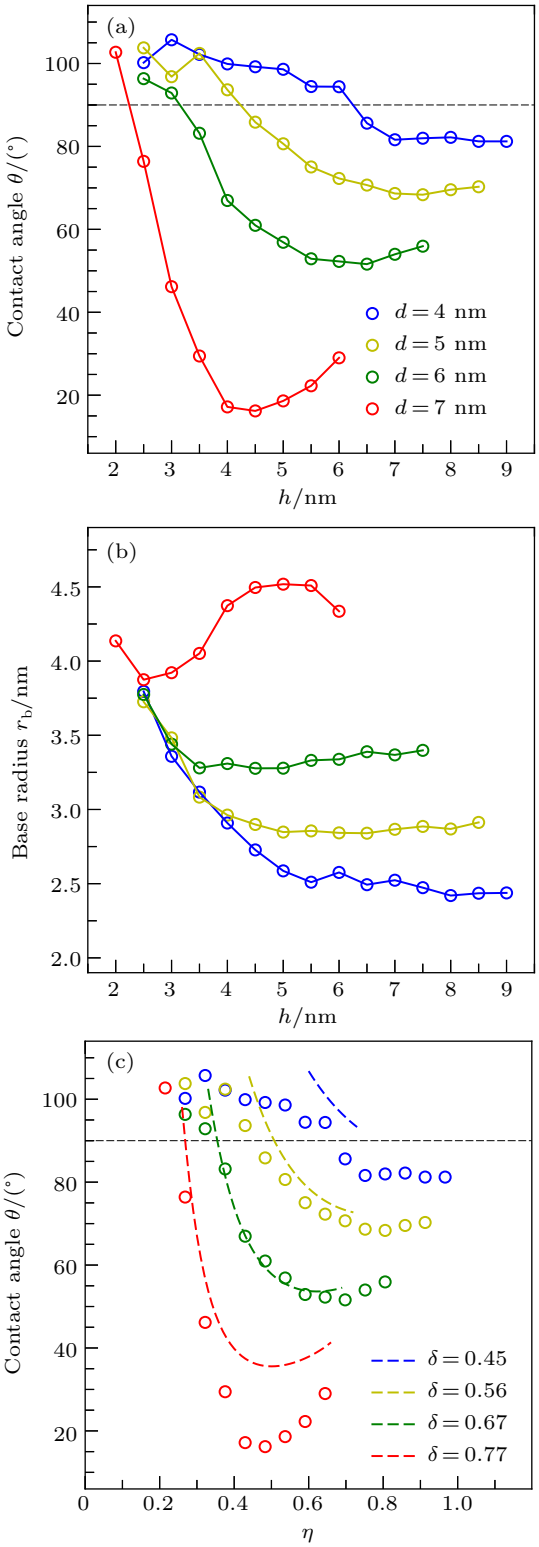

Fig. 3. (a) Contact angle θ and (b) radius of the capillary bridge base radius r_b (see Fig. 1(d)) as function of the wall separations h and for different surface patch diameters d. The profiles of the water capillary bridges are shown in Fig. 2. (c) $\theta(\eta)$ for different δ, where $\eta = \frac{h}{2V^{1/3}}$, $\delta = \frac{r_b}{V^{1/3}}$, and V and r_b are the volume and base radius of the bridge, respectively. Data are obtained from recalculation of (a) (circle) and from macroscopic CT prediction (dashed lines). δ are calculated at $V = 101$ nm^3 and $r_b = d/2 + 0.1$ nm where d corresponds to the patch size. The horizontal dashed line corresponds to $\theta = 90°$ and separates the hydrophobic-like ($\theta > 90°$) and hydrophilic-like ($\theta < 90°$) contact angles.

The data shown in Figs. 2 and 3 extends up to the maximum walls separation h_{br} at which the WCB remains stable. At $h > h_{br}$, the WCB breaks into two droplets, one droplet attached to the patch of each of the walls. Interestingly, h_{br} decreases as the patch size increases. For $d = 4$ nm, the bridge does not break even at $h = 9.5$ nm (after 5 ns relaxation). This value of h_{br} is considerably larger than the value of h_{br} obtained in the presence of homogeneous surfaces with water contact angles in the range from $\theta = 20°$ to $\theta = 108°$, $h_{br} = 7.5$ nm. It follows that the presence of the hydrophilic path enhances the stability of the WCB at large walls separations.

3.2. Force induced by the capillary bridge on the walls

According to capillarity theory, the force exerted by the WCB on the confining surfaces is given by

$$F = 2\gamma\pi\left(r_b \sin\theta - r_b{}^2 H\right), \tag{2}$$

where $\gamma = 0.054 \pm 0.001$ N/m is the liquid–vapor surface tension of water. In this expression, F is negative (positive) if the force between the two surfaces is attractive (repulsive). Figure 4(a) shows the behavior of $F(h)$ obtained from our MD simulations (symbols) together with the corresponding prediction from capillarity theory, Eq. (2), using values of r_b and H obtained independently from Fig. 2. The forces obtained from the MD simulations are in remarkable agreement with capillarity theory for $h > 2.5$ nm. We note that the contributions from the liquid–vapor–solid line tensions are not included. Very minor deviations in the forces obtained from MD simulation and capillarity theory are observed at $h < 3.5$ nm.

Capillarity theory also states that the force F acting on the walls has two components

$$F = F_\gamma + F_P, \tag{3}$$

where $F_\gamma = 2\pi r_b \gamma \sin\theta$ is the force due to the liquid–vapor interface, and $F_P = -2\pi r_b^2 \gamma H$ is the contribution due to the Laplace pressure within the WCB. F_γ and F_P are included in Figs. 4(b) and 4(c). Interesting, while F_γ is always negative (attractive wall–wall interactions), F_P can be either negative or positive (attractive or repulsive) depending on h and the patch size. This is why the total force $F(h)$ is so large for $d = 7$ nm, relative to the case of patches with $d < 7$ nm since only for $d = 7$ nm one finds that $F_P(h) < 0$ (for approximately $h > 2.5$ nm).

3.3. Potential energy stored in the water capillary bridge

Since the force $F(h)$ induced on the surfaces is negative for all WCB studied (Fig. 4(a)), then the WCB can be thought of some kind of (non-linear) spring that is being stretched. Thus, potential energy can be stored in the WCB by changing the wall separation h. The potential energy stored in the bridge, $E_P(h)$, is given by

$$E_P(h) - E_P(h_1) = -\int_{h_1}^{h} F(h')\,\mathrm{d}h', \tag{4}$$

where $E_P(h_1)$ and h_1 are the reference values; we choose $E_P(h_1) = 0$ for $h_1 = 2.5$ nm, and $F(h)$ is the force data obtained from MD simulations after cubic interpolating.

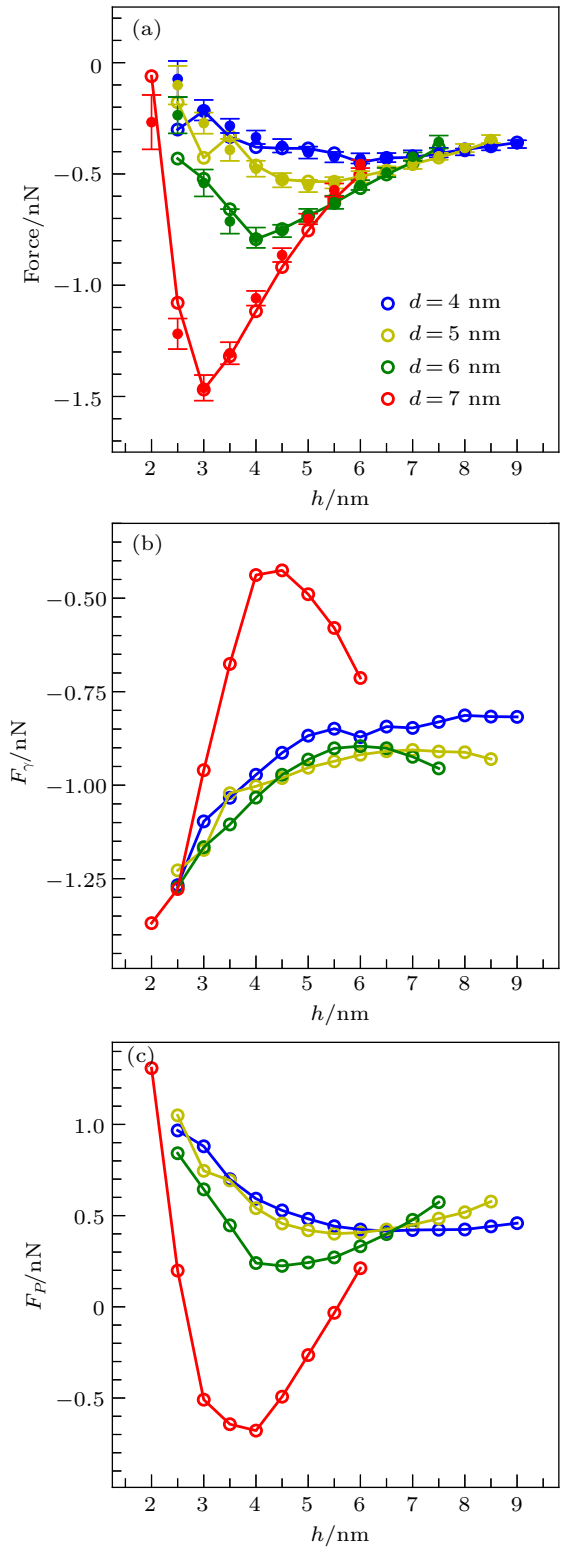

Fig. 4. (a) Force exerted by the water capillary bridges on the confining surfaces as function of separation h obtained from the MD simulation (solid circles with error bars). Lines are the corresponding predictions for the forces on the walls from capillary theory. Positive (negative) values correspond to repulsive (attractive) forces between the surfaces. (b) and (c) Capillarity theory states that the force acting on the walls has two contributions, a force component due to the water–vapor surface tension, $F_\gamma(h)$, and another component due to the pressure of water within the capillary bridge, $F_P(h)$.

Figure 5 shows $E_P(h)$ for the different patch sizes considered. The larger the size of the bridge, the more potential energy is stored in WCB; hence, the maximum potential energy is obtained for the path diameter $d = 7$ nm. This is because for large enough patches, the WCB profiles are always concave (the water contact angle is hydrophilic-like, $\theta < 90°$), implying that the pressure within the WCB is negative (see Fig. 2(d)). This implies that $F_P < 0$ for approximately $h > 2.5$ nm (see Fig. 4(c) and Subsection 3.2). Since $F_\gamma < 0$ for all values of h and d studied, it follows that F_P and F_γ both contribute to make $F(h)$ a net attractive (negative) force, maximizing the $E_P(h)$. Instead, for patches with $d < 7$ nm, this is not the case and the signs of F_γ and F_P not always coincide.

For comparison, we also calculate the potential energy (E_P) stored in AS WCB formed between homogeneous surfaces with different hydrophobicity/hydrophilicity characterized by water contact angles $\theta = 20°, 30°, 60°, 80°, 108°$. This is done by using capillary theory (since it works for $h >$ 2.5 nm). The values of E_P are given in Table 1 and correspond to the wall separation varying from $h = 2,5$ nm to h_{br}. We find that the WCB formed between homogeneous surfaces can store comparable, and even more, potential energy compared to the WCB formed between our patchy surfaces. We note, however, that chemically homogeneous surfaces cannot be used to design energy storing devices. An energy storing device based on the formation of WCB should contain a large number of WCB in close proximity with one another. In the case of homogeneous surfaces, WCB can diffuse along the confining surfaces and hence, they may coalesce. This would reduce the energy storage in the WCBs. Instead, in the case of chemically heterogeneous surfaces with numerous distributed hydrophilic patches, the WCB remain pinned at the surface patches, thus avoiding the WCB diffusion.

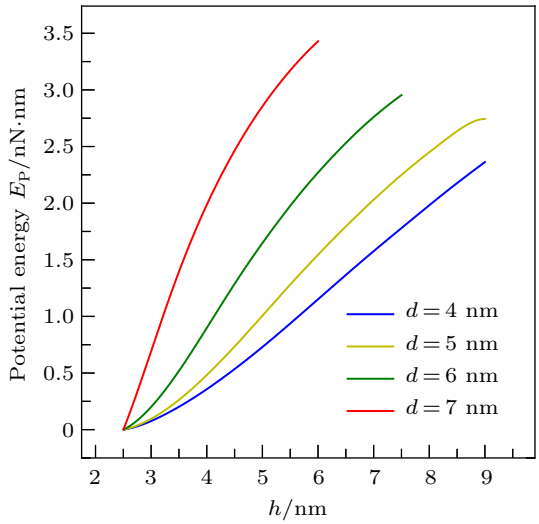

Fig. 5. Potential energy E_P stored in the water capillary bridge as function of the wall separation h. Results are included for all surface patch diameters d studied and for all values of h at which the water capillary bridge remains stable.

Table 1. Potential energy E_P and potential energy density ρ_E stored in AS WCB formed between (a) homogeneous surfaces and (b) chemically heterogeneous surfaces. The homogeneous surfaces are characterized by a water contact angle $\theta = 20°, 30°, 60°, 80°$, and 108°. The heterogeneous surfaces are hydrophobic ($\theta = 108°$) and are decorated by circular patches of diameter $d = 4$ nm, 5 nm, 6 nm, 7 nm (see Fig. 1). In all cases, the calculations of E_P and ρ_E correspond to increasing the wall separations from $h = 2.5$ nm to h_{br}.

	θ	20°	30°	60°	80°	108°
Homogeneous surfaces	potential energy/nN·nm	3.90	4.11	3.88	3.00	1.24
	energy density/kJ·m^{-3}	4991.05	5488.19	5017.96	4000.80	1806.21
	patch diameter	$d = 4$ nm	$d = 5$ nm	$d = 6$ nm	$d = 7$ nm	
Patchy surfaces	potential energy/nN·nm	2.36	2.74	2.95	3.43	
	energy density/kJ·m^{-3}	2722.36	3200.76	4220.97	5715.18	

We also calculate the energy density, $\rho_E = E_P/V_0$, where V_0 is a small volume that is just large enough for the capillary bridge to undergo stretching from $h = 2.5$ nm to h_{br}. The underlying idea is to design a device composed of two identical surfaces that contain a large number of circular patches so many WCBs can be formed between the surfaces. For such a device to function, the WCBs should be separated far enough so they cannot coalesce with one another. Hence, we can estimate V_0 as a cuboid with base $2(r_{max} + 1\ \text{nm}) \times 2(r_{max} + 1\ \text{nm})$ and height h_{br}, i.e.,

$$V_0 = 4h_{br}\,(r_{max} + 1)^2, \tag{5}$$

where r_{max} is the maximum WCB radius $r(z)$. The energy density of AS capillary bridges is presented in Table 1. For different sizes of patches, the energy density follows similar trend as the potential energy. For homogeneous surfaces, the energy density shows a maximum value of 5488 kJ/m^3 at $\theta = 30°$. Considering the pining effect and depletion layer of the surfaces, we approximate $r_{max} = 4$ nm; see Fig. 3(b). We get that the energy density for $d = 7$ nm is about 5715 kJ/m^3. This is the largest among different conditions (both homogeneous and heterogeneous surface). For comparison, we also calculate the energy density of translational symmetric (TS) bridge studied in Ref. [13] with

$$V_0 = 2h_{br}(r_{max} + 1)L, \tag{6}$$

where $2r_{max}$ is the maximum width of the TS WCB at all accessible wall separations, and L is the length of the TS bridge (same as the simulation box side length). As shown in Tables 1 and 2, TS WCB has larger energy density compared to AS WCB, regardless of homogeneous or heterogeneous surfaces. This is due to the smaller volume for energy storage required. We point out that despite of surface properties and shape of the bridge (translational symmetric or axis symmetric), the energy density of the capillary bridge is about 1000–10000 kJ/m^3, which is comparable to that of the water-responsive materials.[23] For instance, ρ_E of carbon nanotube yarn muscles is 1800 kJ/m^3,[36] suggesting that the system based on nanoscale WCB can be useful for designed of nanoscale engines or power generators.

Table 2. Potential energy density ρ_E stored in translationally symmetric WCB expanding between heterogeneous surfaces with stripe-like hydrophilic patches (from Ref. [13]). For comparison, we also include the ρ_E for TS WCB (of the same volume) formed between homogeneous surfaces characterized by water contact angles $\theta = 40°$, 90°, and 108°.

	Stripe	40°	90°	108°
Energy density/kJ·m^{-3}	7563.93	10519.13	6332.27	4054.71

4. Summary

We investigated the properties of WCB confined between heterogeneous surfaces decorated with circular patches of diameter $d = 4$–7 nm. We find that the macroscopic capillarity theory successfully applies to the case of nanoscale WCB, even for the case of very small patch dimensions ($d = 4$ nm) and walls separations $h = 2.5$ nm. Our MD simulations show that, upon stretching the WCB, the contact angle of the WCB changes dramatically, from hydrophobic-like ($\theta > 90°$) to hydrophilic-like values ($\theta < 90°$). This is in contrast to the case of WCB confined by homogeneous surfaces where θ remains constant, independent of h. Due to the presence of surface hydrophilic patches, the WCB remain stable for up to large wall separations (e.g., $h_{br} = 9.5$ nm), larger than the maximum wall separations accessible in the case of homogeneous surfaces ($h_{br} = 7.5$ nm).[28] We also study the potential energy that our WCB can store. We find that the maximum stored potential energy is obtained when the force due to the liquid–vapor surface tension (F_γ) and the Laplace pressure force (F_P) are both parallel and negative (attractive). This is the case of our large hydrophilic patch with $d = 7$ nm. This can be achieved by requiring that the contact angle of the WCB is hydrophilic-like ($\theta < 90°$) at small h. At the same time, one should consider small surface patches in order to minimize volume occupied by the WCB. Circular (AS WCB) as well as stripe-like patches (TS WCB) are both suitable surface patch shapes that can be used to store relevant potential energies in WCB. Our results show that nanoscale WCB can be exploited for the design of energy storage devices and water responsive systems/materials for energy conversion and energy harvesting applications.[23] These finding can be of importance to different scientific and engineering applications, including the design of water responsive materials for energy storage devices, power generators, and actuators.[37,38]

Acknowledgment

We are grateful for computational resources provided by the supercomputer TianHe-1A in Tianjin and the High Performance Computing Platform of Peking University, China.

References

[1] Harrison A J, Beaudoin S P and Corti D S 2016 *J. Adhes. Sci. Technol.* **30** 1165
[2] Wei Z, Sun Y, Ding W X and Wang Z R 2016 *Sci. China-Phys. Mech. Astron.* **59** 694611
[3] Lai T and Li P 2019 *Langmuir* **35** 6585
[4] Anzivino C, Chang F Q, Soligno G, Roij R V, Kegelb W K and Dijkstra M 2019 *Soft Matter* **15** 2638
[5] Shi S and Russell T P 2018 *Adv. Mater.* **30** 1800714
[6] Mayer R P and Stowe R A 2005 *J. Colloid Interface Sci.* **285** 781
[7] de Boer P C T and de Boer M P 2008 *Langmuir* **24** 160
[8] Dodds S, Carvalho M S and Kumar S 2011 *Langmuir* **27** 1556
[9] Goegelein C, Brinkmann M, Schroeter M and Herminghaus S 2010 *Langmuir* **26** 17184
[10] Valenzuela G E 2019 *J. Phys. Chem. C* **123** 1252
[11] Saavedra J H, Rozas R E and Toledo P G 2014 *J. Colloid Interface Sci.* **426** 145
[12] Yaneva J, Milchev A and Binder K 2004 *J. Chem. Phys.* **121** 12632
[13] Tang B Z, Buldyrev S V, Xu L M and Giovambattista N 2020 *Langmuir* **36** 7246
[14] de Gennes P, Brochard-Wyart F and Queéré D 2004 *Capillarity and Wetting Phenomena: Drops, Bubbles, Pearls, Waves*
[15] Alencar A M, Wolfe E and Buldyrev S V 2006 *Phys. Rev. E* **74** 026311
[16] Almeida A B, Giovambattista N, Buldyrev S V and Alencar A M 2018 *J. Phys. Chem. C* **122** 1556
[17] Swain P S and Lipowsky R 2000 *Europhys. Lett.* **49** 203
[18] Schoen M and Diestler D J 1997 *Chem. Phys. Lett.* **270** 339
[19] Iwamatsu M 2007 *Langmuir* **23** 11051
[20] Hwang S H, Lee J and Khang D Y 2019 *ACS Appl. Mater. Interfaces* **11** 8645
[21] Wu C C, Reinhoudt D N, Otto C, Subramaniam V and Velders A H 2011 *Small* **7** 989
[22] Mariappan D D, Kim S, Boutilier M S H, Zhao J J, Zhao H B, Beroz J, Muecke U, Sojoudi H, Gleason K, Brun P T and Hart A J 2019 *Langmuir* **35** 7659
[23] Chen X, Goodnight D, Gao Z, Cavusoglu A H, Sabharwal N, DeLay M, Driks A and Sahin O 2015 *Nat. Commun.* **6** 7346
[24] Liu B, Qi C, Zhao X, Teng G, Zhao L, Zheng H, Zhan K and Shi J 2018 *J. Phys. Chem. C* **122** 26671
[25] Xiong H, Devegowda D and Huang L L 2020 *Langmuir* **36** 723
[26] Giovambattista N, Rossky P J and Debenedetti P G 2006 *Phys. Rev. E* **73** 041604
[27] Berendsen H J C, Grigera J C and Stroatsma T P 1987 *J. Phys. Chem.* **91** 6269
[28] Giovambattista N, Almeida A B, Alencar A M and Buldyrev S V 2016 *J. Phys. Chem. C* **120** 1597
[29] Giovambattista N, Debenedetti P G and Rossky P J 2007 *J. Phys. Chem. B* **111** 9581
[30] Plimpton S 1995 *J. Comput. Phys.* **117** 1
[31] Werder T, Walther J H, Jaffe R L, Halicioglu T and Koumoutsakos P 2003 *J. Phys. Chem. B* **107** 1345
[32] Broesch D J and Frechette J 2012 *Langmuir* **28** 15548
[33] Giovambattista N, Debenedetti P G and Rossky P J 2007 *J. Phys. Chem. C* **111** 1323
[34] Vogel T I 1987 *SIAM J. Appl. Math* **47** 516
[35] Vogel T I 1989 *SIAM J. Appl. Math* **49** 1009
[36] Kim S H, Kwon C H, Park K, Mun T J, Lepro'o X, Baughman R H, Spinks G M, and Kim S J 2016 *Sci. Rep.* **6** 23016
[37] Cavusoglu A, Chen X, Gentine P and Sahin O 2017 *Nat. Commun.* **8** 617
[38] Xu W, Zheng H, Liu Y, Zhou X F, Zhang C, Song Y X, Deng X, Leung M, Yang Z B, Xu R X, Wang Z L, Zeng X C and Wang Z K 2020 *Nature* **578** 392